Canadian Science Publishing | Transactions of the Canadian Society for Mechanical Engineering

Creep Prediction of GFRP Directors in Multiple Launch Rocket System under Long-term Stacking Storage

Journal:	*Transactions of the Canadian Society for Mechanical Engineering*
Manuscript ID	TCSME-2020-0021.R1
Manuscript Type:	Article
Date Submitted by the Author:	15-Mar-2020
Complete List of Authors:	Sun, Tong-Sheng; Nanjing University of Science and Technology, School of Mechanical Engineering Yu, Cun-Gui; Nanjing University of Science and Technology, Wang, Qi; Jiangxi Changjiang Chemical Co. Ltd. Zhong, Jian-Lin; Nanjing University of Science and Technology School of Mechanical Engineering
Keywords:	composite directors, nonlinear viscoelasticity, long-term storage, creep deformation, finite-element analysis
Is the invited manuscript for consideration in a Special Issue? :	Not applicable (regular submission)

Creep Prediction of GFRP Directors in Multiple Launch Rocket System under Long-term Stacking Storage

Tong-Sheng Sun[1], Cun-Gui Yu[1], Qi Wang[2], Jian-Lin Zhong[1],

[1]*School of Mechanical Engineering, Nanjing University of Science and Technology, Nanjing 210094, Jiangsu, China*

[2]*Jiangxi Changjiang Chemical Co. Ltd., 1210# East of Qianjin Road, Jiujiang 332006, China*

Corresponding author：

Name: Cun-Gui Yu

Address: No. 200, XiaoLingWei Street, XuanWu District, Nanjing, Jiangsu, China.

Telephone numbers: +86 13851711833

E-mail addresses: yu-cungui@njust.edu.cn

Abstract

During long-term stacking storage, creep deformation of polymeric composite directors used in multiple launch rocket system can appears, which affects rocket launch. In this work, E-glass/epoxy 6509 composite laminates were prepared and the 60/60-minute creep/creep-recovery tests were carried out in the transverse and shear directions at different stress levels. Parameters of the Schapery's nonlinear viscoelastic equation were obtained based on the test data. Then, a three-dimensional nonlinear viscoelastic constitutive model based on Schapery's equation was implemented in the standard finite element code UMAT and a finite element model was developed to predict the creep deformation of the composite directors after 15 years of stacking storage. The effect of creep deformation on rocket launching was also studied The results show that the residual deformation of the directors is a saddle-shaped distribution in three-dimensional space, the maximum residual deformation is 0.24 mm, and the minimum residual deformation is 0.22 mm. The creep deformation of the director causes a significant increase in the contact-collision force during launching, resulting in a decrease in the rocket run-off track velocity.

Keywords: composite directors; nonlinear viscoelasticity; long-term storage; creep deformation; finite-element analysis

1. Introduction

The multiple launch rocket system (MLRS) plays an increasingly important role in modern warfare due to its strong firepower, high flexibility and long-range precision strikes. In order to further improve the mobility and rapid response capability of MLRS and achieve the goal of "multi-skill and multi-purpose", a modular launch canister, clustering of E-glass fiber/epoxy composite (GFRP) directors, is generally equipped (Yu and Li 2012). However, polymeric composites are known to exhibit a time-dependent behavior due to the viscoelastic properties of the polymers, and the GFRP director undergoes creep deformation during long-term (15 years) stacking storage. Deformation of the director has a negative impact on launch safety and firing dispersion. Therefore, it is necessary to investigate the creep behavior of the director and evaluate its long-term service performance. In a recent work (Yu et al. 2019), the authors studied the creep deformation of the steel frame of the launch canister but did not consider the creep response of the GFRP director.

Studies have shown that there is a stress threshold beyond which the polymers and polymeric composites exhibit nonlinear viscoelastic characteristics (Tuttle and Brinson 1986). Many theoretical models have been proposed to describe the nonlinear viscoelastic response of materials, and the most widely used is the well-known Schapery single integral nonlinear viscoelastic model (Schapery 1968a; 1969b) According to this model, the nonlinear viscoelasticity of a material is controlled by four parameters, g_0, g_1, g_2 and a_σ, depending on stress, temperature and moisture, which reflect the deviation from the linear viscoelastic response (Papanicolaou et al. 1999). Transient creep compliance, usually represented by a power law model (Rariee R and Mazhari 2015) or a generalized Kelvin model (Guedes 2010), is also used in the Schapery model.

The relationship between these nonlinear parameters and stress is a key issue to be solved by applying the Schapery model After performing a series of short-term (on the order of hours) creep/creep-recovery tests at different stress levels, the nonlinear parameters can be identified by the least-squared-error method (Tuttle and Brioson 1986), graphical method (Hiel et al. 1983) and analytical method (Papanicolaou et al. 1999; Zaoutsos et al. 1998). Among them, the analytical method only needs to determine the critical time point according to the original creep/recovery strain

curves, such as the creep starting and ending points and the recovery starting points, and the nonlinear parameters can be determined conveniently and quickly. Therefore, the analytical method is used in present study.

The goal of theoretical and experimental research is to predict the long-term viscoelastic response of any laminate composite and its structures. Dillard et al. (1981) developed a Fortran computer code (VISLAP) for predicting creep and creep rupture of any laminates based on the classical lamination theory (CLC), the Findley MSP, the modified form of the Tsai-Hill failure criteria, and the cumulative damage law. Tuttle and Brinson (1986) presented a modified version of VISLAP to predict the creep response of multi-directional laminate composites. Guedes et al. (2010) developed a computer program (RESFLU) based on the Schapery's nonlinear viscoelastic model to predict the long-term creep behavior of thick-walled cylindrical composite pipes. Rafiee et al. (2015) developed a comprehensive model for evaluating the creep response of any composite structure. The time-temperature superposition principle (TTSP), Schapery's nonlinear viscoelastic model and micromechanics theory were included in the comprehensive model. Haj-Ali and Muliana (2004) and Behzadpoor et al. (2011) developed a multi-scale finite element method for predicting long-term nonlinear viscoelasticity of fiber reinforced composites based on micromechanics theory. Schapery integral was used to account for the nonlinear viscoelasticity of epoxy matrix and assumed that the compliance of the fiber is time independent. Chen et al. (2013) predicted the creep deformation of the polymeric composite pipes after 50 years of service, based on the double shift factor method.

The main objective of this work is to evaluate the long-term storage creep response of composite directors in multiple launch rocket systems. E-glass/epoxy 6509 composite laminates were prepared and subjected to 60/60-minute creep/creep-recovery tests for $[90]_{16}$ and $[\pm 45]_{4S}$ specimens at different stress levels. The Schapery's nonlinear parameters were obtained as a function of the average matrix octahedral shear stress. The master curves of long-term creep compliance for the transverse and shear directions were developed based on the TSSP, and the linear transient creep compliance in Prony series was obtained by a curve fitting procedure. A three-dimensional nonlinear viscoelastic constitutive model based on Schapery's equation was implemented in the standard finite

element code UMAT, and a finite element model for predicting creep deformation of composite directors under long-term stacking storage was established. Furthermore, the effect of creep deformation on rocket launching was also studied.

2. Theoretical background

2.1 Schapery model and parameters identification method

Schapery developed a single integral constitutive equation based on irreversible thermodynamics for predicting the nonlinear viscoelastic behavior under isothermal and uniaxial loading conditions, as shown below (Schapery 1966):

$$\varepsilon^t = g_0 D_0 \sigma^t + g_1 \int_0^t \Delta D(\psi^t - \psi^\tau) \frac{\partial}{\partial \tau}\left[g_2 \sigma^\tau \right] d\tau \tag{1}$$

where $\Delta D(\psi)$ is the linear transient creep compliance and ψ^t is the reduced-time defined by eqs. (2) and (3):

$$\psi^t = \int_0^t \frac{d\xi}{a_\sigma \left[\sigma(\xi)\right]} \tag{2}$$

$$\psi^\tau = \int_0^\tau \frac{d\xi}{a_\sigma \left[\sigma(\xi)\right]} \tag{3}$$

The factor g_0 indicates the nonlinearity of the instantaneous elastic compliance due to stress and temperature changes, which can be obtained by comparing the instantaneous compliance value in the nonlinear case with the instantaneous compliance value in the linear case. Factor g_1 has a similar interpretation but acts on transient creep compliance, while g_2 shows the effect of loading rate on nonlinearity (Papanicolaou et al. 1999). The factor a_σ is a time shift factor that indicates the acceleration effect of high stress level on creep. When all parameters are equal to one, the constitutive equation described by eq. (1) is simplified to the case of linear viscoelasticity.

Zaoutsos and Papanicolaou et al. (1998a, 1999b, and 1999c) proposed a modified Schapery equation by introducing additional viscoplastic strain components, and gave an analytical expression for solving g_1 and g_2, as follows:

$$g_1 = \frac{\Delta\varepsilon_c - \varepsilon_{vp}}{\Delta\varepsilon_c - \Delta\varepsilon_0 - \varepsilon_{vp}} \tag{4}$$

$$g_2 = \frac{\Delta\varepsilon_{0(nl)}}{\Delta\varepsilon_{c(l)}} \frac{a_\sigma^m}{(g_1 - 1)} \frac{\sigma_{0(l)}}{\sigma_{0(nl)}} \tag{5}$$

where m is the time exponent of the power law model (Guedes 2010). $\Delta\varepsilon_c$, $\Delta\varepsilon_0$ and ε_{vp} represent the creep strain, the difference between the instantaneous unloading strain and the instantaneous loading strain, and the residual viscoplastic strain component at the end of the creep/creep-recovery test, respectively. The indices *l* and *nl* denote the magnitudes associated with linear and nonlinear viscoelastic response, respectively.

Equation (5) shows that the factor g_2 is related to the time exponent m and the time shift factor a_σ, therefore, the values of m and a_σ should be determined firstly. The time exponent m can be estimated by numerically fitting the recovery strain data in the linear case. Similarly, the determination of a_σ can be performed by fitting the recovery strain data in the nonlinear case.

2.2 Generalized Kelvin model for linear creep compliance

The generalized Kelvin model can be understood by first looking at a single Kelvin element, which consists of a linear spring and a dashpot in parallel (Gramoll et al. 1989). The creep strain response of a single Kelvin element under step stress $\sigma=\sigma_0 H(t)$ is given by:

$$\varepsilon^t = \sigma_0 D(1 - e^{-\lambda t}) \tag{6}$$

where $H(t)$ is the well-known Heaviside unit-step function, $D = 1/E$, $\lambda = E/\eta$. E and η are the spring constant and the dashpot viscosity, respectively.

The creep compliance function D_c^t is obtained from eq. (6) by dividing the left hand of the equation by σ_0, giving

$$D_c^t = D(1 - e^{-\lambda t}) \tag{7}$$

However, in order to accurately describe the long-term creep response of a material, a generalized Kelvin model is usually constructed in series using several single Kelvin elements and a Maxwell model (Yang et al. 2004), as shown in Fig. 1.

The creep compliance of the generalized Kelvin model is as follows:

$$D_c^t = D_0 + \sum_{n=1}^{N} D_n(1-e^{-\lambda_n t}) + D_f t \tag{8}$$

where N is the number of Kelvin elements, generally $N \geq 6$; D_0 is the instantaneous linear viscoelastic creep compliances, and $D_f t$ represents a steady flow component. $D_0 = 1/E_0$, $D_n = 1/E_n$, $\lambda_n = E_n/\eta_n$, $D_f = 1/\eta_0$.

From eq. (8), we can get a linear-transient creep compliance expressed as a Prony series plus a steady flow component:

$$\Delta D(\psi^t - \psi^\tau) = \sum_{n=1}^{N} D_n[1-e^{-\lambda_n t(\psi^t-\psi^\tau)}] + D_f(\psi^t - \psi^\tau) \tag{9}$$

The Prony series in eq. (9) contains many unknown material parameters, two parameters for each Kelvin element are required. It is necessary to extend the time scale of the test data as much as possible for determining these parameters accurately. Therefore, a master curve of long-term creep compliance is obtained from the short-term compliance based on the TTSP (time-stress superposition principle (TSSP) (Guedes et al. 2010) used in present study, see in Section 4.2), and these parameters are determined by a numerical curve fitting procedure.

3 Experimental procedures

3.1 Materials, equipment and method

The manufacture of the specimens was carried out in Jiangxi Changjiang Chemical Co., Ltd. Specimens with 0- ,90-, and ± 45-deg fiber orientations were cut from 16-ply E-glass/epoxy 6509 composites panels. These panels were fabricated by the hand lay-up technique using a standard prepreg type G20000 with a nominal weight of 0.2kg/m^2, a nominal thickness of 0.17mm, and a fiber volume fraction of 65%. After 120 minutes of curing cycle consisting of a pressure of 2 MPa and a curing temperature of 120°, all panels were cured in an autoclave and then slowly cooled to room temperature while maintaining pressure. The specimens were cut from the current panels using a diamond wheel saw. The nominal specimen lengths are 250 mm (10.0 in.) for 0- and ± 45-deg

specimens and 175 mm (7.0 in.) for 90-deg specimens, respectively. The nominal specimen widths are 15 mm (0.60 in.) for 0-deg specimens and 25 mm (1.0 in.) for 90- and $\pm$45-deg specimens, respectively. The nominal thickness is 2.0 mm (0.08 in.).

A quasi-static tensile test should be carried out to determine the elastic modulus and ultimate strength of the specimens to provide a reference for the reasonable selection of the stress levels in creep/creep-recovery test. The stress level applied in the creep test should be between 10% and 80% of the ultimate strength (Japanese Standards Association 1996). Quasi-static tests were carried out at a loading rate of 2 mm/min. Elastic properties were measured as shown in Table 1.

The 60/60-minute creep/creep-recovery tests were carried out in the transverse and shear directions at room temperature while assuming time-independent properties in the fiber direction. The recorded strain data has seven stress levels in the transverse direction ranging from 17MPa to 35MPa, and eight stress levels in the shear direction ranging from 9MPa to 30MPa. Due to the limitation of the force sensor, a load was applied within 8s with the maximum allowable loading speed of 500N/s, and the loading time was short compared to the creep test period of 60 minutes. Quasi-static tests and creep/creep-recovery tests were carried out on the UTM5105-G electronic universal material testing machine. Strain data was measured and recorded by BF120-3AA strain gages, YE3818C dynamic strain amplifier, YE29003A bridge box and NI9215 data collector. In order to eliminate the influence of moisture on the viscoelasticity of the composites, the samples were dried at a drying temperature of 50°C for 72h to a constant weight prior to bonding the strain gauges. In addition, a temperature compensator was used to eliminate strain measurement error caused by changes in ambient temperature.

3.2 Nonlinear parameters as a function of stress

Figure 2 shows the 60/60-minute creep/creep-recovery strain versus time curves at different stress levels in the transverse and shear directions. As expected, the E-glass/epoxy 6509 composite exhibits strong viscoelastic behavior in both directions. It can also be seen from these figures that there is a stress threshold and that the E-glass/epoxy 6509 composite exhibits a nonlinear viscoelasticity when the applied stress is above this value. During the tests, the ambient temperature and humidity were

monitored by an electronic thermo-hygrometer to ensure that the nonlinear viscoelasticity was only caused by stress changes.

The isochronous curves shown in Fig. 3 denote that the nonlinear viscoelastic response occurs when the stress applied in the transverse direction is higher than 26MPa, and the nonlinear viscoelastic stress threshold in the shear direction is 15MPa.

According to the identification method mentioned in Section 2.1, the calculated values of the nonlinear parameters are presented in Fig. 4, which are functions of both the applied stress and the average matrix octahedral shear stress, τ_{oct} (Huang et al. 2007). In Fig. 4, the subscript *T* refers to a transverse parameter, and the subscript *S* refers to a shear parameter.

According to the parameters values shown in Fig. 4(a), it can be observed that g_{1T} value increases as the stress level increase, while the $a_{\sigma T}$ value decreases as the stress level increases, and the values of g_{0T} and g_{2T} are independent of the stress level. In the shear direction shown in Fig. 4(b), the value of g_{0S} increases as the stress level increases, indicating that the instantaneous elastic compliances exhibits nonlinearly, and material softening occurs. The g_{1S} and g_{2S} values show the same variation as g_{0S} and the $a_{\sigma S}$ values show the same variation as $a_{\sigma T}$, which means that the stress has a significant accelerate effect of viscoelasticity in both the transverse direction and shear directions.

An expression for each parameter as a function of τ_{oct} is required for numerical simulation. All parameters of the transverse direction and the parameters g_{1S} and $a_{\sigma S}$ of the shear direction were fitted with the simple bi-linear expressions, while the parameters g_{0S} and g_{2S} were fitted by an exponential function. These expressions are presented in Table 2.

3.3 Parameters for linear transient creep compliance

Based on the TSSP, The master curves of long-term creep compliance for both transverse and shear directions were developed, as shown in Fig. 5. Due to the logarithmic time axis, it is difficult to directly fit the master curves by eq. (8). Therefore, using a transformation method with the power law model to approximate the master curves, and then we converted the power law to the Prony series through curve-fitting technique based on the Levenberg-Marquardt least squares method (Gallant 1987) used by Tuttle and Brinson (1986). The parameters for linear transient creep compliance are

given in Table 3.

4 Prediction of creep deformation for composite directors

4.1 Implementation of nonlinear viscoelastic constitutive in FEM

In order to quantify the nonlinear viscoelastic constitutive equations into a finite element framework, the Schapery integral equation was converted into an incremental iteration form (Kennedy and Wang 1994). The detailed derivation is as follows.

Substituting eq. (9) into eq. (1) and expanding the integral term gives

$$\varepsilon^t = g_0^t D_0 \sigma^t + g_1^t g_2^t \sigma^t \sum_{n=1}^{N} D_n - g_1^t \int_0^t \sum_{n=1}^{N} D_n e^{-\lambda_n (\psi^t - \psi^\tau)} \frac{\partial}{\partial \tau}(g_2^\tau \sigma^\tau) d\tau + g_1^t D_f \int_0^t (\psi^t - \psi^\tau) \frac{\partial}{\partial \tau}(g_2^\tau \sigma^\tau) d\tau \quad (10)$$

As mentioned earlier, the nonlinear parameters are a function of stress, so they are also time-dependent. The superscript t refers to time-dependence. Generalizing eq. (10) to three dimensions gives

$$\varepsilon_i^t = \sum_{j=1}^{6} \Bigg[g_{0,ij}^t D_{0,ij} \sigma_j^t + g_{1,ij}^t g_{2,ij}^t \sigma_j^t \sum_{n=1}^{N} D_{n,ij} - g_{1,ij}^t \int_0^t \sum_{n=1}^{N} D_{n,ij} e^{-\lambda_{n,ij} (\psi_{ij}^t - \psi_{ij}^\tau)} \frac{\partial}{\partial \tau}\left(g_{2,ij}^t \sigma_j^t\right) d\tau$$

$$+ g_{1,ij}^t D_{f,ij} \int_0^t (\psi_{ij}^t - \psi_{ij}^\tau) \frac{\partial}{\partial \tau}(g_{2,ij}^\tau \sigma_j^\tau) d\tau \Bigg] \quad i = 1, 2, ..., 6 \quad (11)$$

where, the reduced time is defined as

$$\psi_{ij}^t = \int_0^t \frac{d\xi}{a_{\sigma,ij}}, \quad \psi_{ij}^\tau = \int_0^\tau \frac{d\xi}{a_{\sigma,ij}} \quad (12)$$

Simplifying the exponential integral term in eq. (11) by a subsection integral method gives

$$q_{n,ij}^t = I_1 + I_2 = \int_0^{t-\Delta t} e^{-\lambda_{n,ij} (\psi_{ij}^t - \psi_{ij}^\tau)} \frac{\partial}{\partial \tau}\left(g_{2,ij}^\tau \sigma_j^\tau\right) d\tau + \int_{t-\Delta t}^t e^{-\lambda_{n,ij} (\psi_{ij}^t - \psi_{ij}^\tau)} \frac{\partial}{\partial \tau}\left(g_{2,ij}^\tau \sigma_j^\tau\right) d\tau \quad (13)$$

Noting that

$$\Delta \psi_{ij}^t = \int_{t-\Delta t}^t \frac{d\xi}{a_{\sigma,ij}} = \psi_{ij}^t - \psi_{ij}^{t-\Delta t} \quad (14)$$

then the first integral term in eq. (13) can be rewritten and simplified as

$$\begin{aligned} I_1 &= e^{-\lambda_{n,ij}\Delta\psi_{ij}^t}\int_0^{t-\Delta t} e^{-\lambda_{n,ij}(\psi_{ij}^t-\Delta\psi_{ij}^t-\psi_{ij}^\tau)}\frac{\partial}{\partial\tau}\left(g_{2,ij}^\tau\sigma_j^\tau\right)d\tau \\ &= e^{-\lambda_{n,ij}\Delta\psi_{ij}^t}\int_0^{t-\Delta t} e^{-\lambda_{n,ij}(\psi_{ij}^{t-\Delta t}-\psi_{ij}^\tau)}\frac{\partial}{\partial\tau}\left(g_{2,ij}^\tau\sigma_j^\tau\right)d\tau \\ &= e^{-\lambda_{n,ij}\Delta\psi_{ij}^t}q_{n,ij}^{t-\Delta t} \end{aligned} \tag{15}$$

The second integral term in eq. (13) can be integrated by parts, as follows

$$I_2 = \frac{a_{\sigma,ij}e^{-\lambda_{n,ij}(\psi_{ij}^t-\psi_{ij}^\tau)}}{\lambda_{n,ij}}\frac{\partial}{\partial\tau}\left(g_{2,ij}^\tau\sigma_j^\tau\right)\Big|_{t-\Delta t}^{t} - \int_{t-\Delta t}^{t}\frac{a_{\sigma,ij}e^{-\lambda_{n,ij}(\psi_{ij}^t-\psi_{ij}^\tau)}}{\lambda_{n,ij}}\frac{\partial^2}{\partial\tau^2}\left(g_{2,ij}^\tau\sigma_j^\tau\right)d\tau \tag{16}$$

Since the nonlinear parameter a_σ is not a direct function of time, and for a sufficiently small time increment Δt, we can assume that $g_{2,ij}^t\sigma_j^t$ is linear over the time period Δt, then

$$\frac{\partial}{\partial\tau}\left(g_{2,ij}^\tau\sigma_j^\tau\right) = Constant, \quad \frac{\partial^2}{\partial\tau^2}\left(g_{2,ij}^\tau\sigma_j^\tau\right) = 0 \tag{17}$$

Calculating eq. (16) according to eq. (17) gives

$$I_2 = \frac{a_{\sigma,ij}e^{-\lambda_{n,ij}(\psi_{ij}^t-\psi_{ij}^\tau)}}{\lambda_{n,ij}}\frac{\partial}{\partial\tau}\left(g_{2,ij}^\tau\sigma_j^\tau\right)\Big|_{t-\Delta t}^{t} = \Gamma_{n,ij}\left(g_{2,ij}^t\sigma_j^t - g_{2,ij}^{t-\Delta t}\sigma_j^{t-\Delta t}\right) \tag{18}$$

where

$$\Gamma_{n,ij} = \frac{\left(1-e^{-\lambda_{n,ij}\Delta\psi_{ij}^t}\right)}{\lambda_{n,ij}\Delta\psi_{ij}^t} = \frac{a_{\sigma,ij}\left(1-e^{-\lambda_{n,ij}\Delta t/a_{\sigma,ij}}\right)}{\lambda_{n,ij}\Delta t} \tag{19}$$

Substituting eq. (15) and eq. (18) into eq. (13), obtains a recursive iterative form of $q_{n,ij}^t$ as

$$q_{n,ij}^t = e^{-\lambda_{n,ij}\Delta\psi_{ij}^t}q_{n,ij}^{t-\Delta t} + \Gamma_{n,ij}\left(g_{2,ij}^t\sigma_j^t - g_{2,ij}^{t-\Delta t}\sigma_j^{t-\Delta t}\right) \tag{20}$$

From the view of numerical calculation, eq. (20) is much easier to handle than eq. (13) because eq. (20) only needs to know the variable information of the current time step t and the previous time step t-Δt, while eq. (13) requires to calculate and store the material response over the entire time history. Therefore, the solution efficiency is significantly improved.

A similar approach can be used to simplify the last integral in eq. (11) given

$$q_{f,ij}^t = q_{f,ij}^{t-\Delta t} + 0.5\Delta\psi_{ij}^t\left(g_{2,ij}^t\sigma_j^t - g_{2,ij}^{t-\Delta t}\sigma_j^{t-\Delta t}\right) \tag{21}$$

According to the above equations, a three-dimensional anisotropic nonlinear creep constitutive

equation in the form of recursive iteration is established.

$$\begin{aligned}\varepsilon_i^t = \sum_{j=1}^{6}\Bigg\{&\left[g_{0,ij}^t D_{0,ij} + g_{1,ij}^t g_{2,ij}^t \sum_{n=1}^{N} D_{n,ij}\left(1-\Gamma_{n,ij}^t\right) + 0.5 g_{1,ij}^t g_{2,ij}^t D_{f,ij}\Delta\psi_{ij}^t \right]\sigma_j^t \\ &+ g_{1,ij}^t g_{2,ij}^{t-\Delta t}\left(\sum_{n=1}^{N} D_{n,ij}\Gamma_{n,ij}^t + 0.5 D_{f,ij}\Delta\psi_{ij}^t \right)\sigma_j^{t-\Delta t} - g_{1,ij}^t\left(\sum_{n=1}^{N} D_{n,ij} e^{-\lambda_{n,ij}\Delta\psi_{ij}^t} q_{n,ij}^{t-\Delta t} - D_{f,ij} q_{f,ij}^{t-\Delta t} \right)\Bigg\}\end{aligned} \tag{22}$$

Equation (22) can be written in matrix form as

$$\{\varepsilon\} = [S]\{\sigma\} + [H] \tag{23}$$

where $[S]$ is the instantaneous compliance matrix, and $[H]$ is the hereditary strain matrix.

$$[H] = [H_A]\left\{\sigma^{t-\Delta t}\right\} + [H_B] \tag{24}$$

However, the finite element software calculates the stress based on the current strain during the calculation, which means that we need to solve for $\{\sigma\}$ in eq. (23) given

$$\{\sigma\} = [S]^{-1}\left(\{\varepsilon\} - [H]\right) \tag{25}$$

For a three-dimensional, transversely isotropic composite layer, there are twelve nonzero terms in the matrix $[S]$ and only five of them are independent. The nonzero terms are given as

$$S_{11} = 1/E_1 \tag{26-1}$$

$$S_{12} = S_{13} = S_{21} = S_{31} = -\upsilon_{12}/E_1 \tag{26-2}$$

$$S_{22} = S_{33} = g_{0,T}^t/E_2 + g_{1,T}^t g_{2,T}^t\left[\sum_{n=1}^{N} D_{n,T}\left(1-\Gamma_{n,T}\right) + D_{f,T}\Delta\psi_T^t\right] \tag{26-3}$$

$$S_{23} = S_{32} = -\upsilon_{23} g_{0,T}^t/E_2 - \upsilon_{23} g_{1,T}^t g_{2,T}^t\left[\sum_{n=1}^{N} D_{n,T}\left(1-\Gamma_{n,T}\right) + D_{f,T}\Delta\psi_T^t\right] \tag{26-4}$$

$$S_{44} = 2(1+\upsilon_{23})S_{22} \tag{26-5}$$

$$S_{55} = S_{66} = g_{0,S}^t/G_{12} + g_{1,S}^t g_{2,S}^t\left[\sum_{n=1}^{N} D_{n,S}\left(1-\Gamma_{n,S}\right) + D_{f,S}\Delta\psi_S^t\right] \tag{26-6}$$

The nonzero terms in matrix $[H_A]$ can be written as

$$\begin{aligned}H_{A22} = H_{A33} &= -H_{A23}/\upsilon_{23} = -H_{A32}/\upsilon_{23} = 0.5H_{A44}/(1+\upsilon_{23}) \\ &= g_{1,T}^t g_{2,T}^{t-\Delta t}\left(\sum_{n=1}^{N} D_{n,T}\Gamma_{n,T} + 0.5 D_{f,T}\Delta\psi_T^t\right)\end{aligned} \tag{27-1}$$

$$H_{A55} = H_{A66} = g_{1,S}^{t} g_{2,S}^{t-\Delta t} \left(\sum_{n=1}^{N} D_{n,S} \Gamma_{n,S} + 0.5 D_{f,S} \Delta \psi_{S}^{t} \right) \tag{27-2}$$

and the nonzero terms in matrix $[H_B]$ can be written as

$$H_{B2} = -g_{1,T}^{t} \left[\sum_{n=1}^{N} D_{n,T} e^{-\lambda_{n,T} \Delta \psi_{T}^{t}} (q_{n,2}^{t-\Delta t} - \upsilon_{23} q_{n,3}^{t-\Delta t}) - D_{f,T} (q_{f,2}^{t-\Delta t} - \upsilon_{23} q_{f,3}^{t-\Delta t}) \right] \tag{28-1}$$

$$H_{B3} = -g_{1,T}^{t} \left[\sum_{n=1}^{N} D_{n,T} e^{-\lambda_{n,T} \Delta \psi_{T}^{t}} (q_{n,3}^{t-\Delta t} - \upsilon_{23} q_{n,2}^{t-\Delta t}) - D_{f,T} (q_{f,3}^{t-\Delta t} - \upsilon_{23} q_{f,2}^{t-\Delta t}) \right] \tag{28-2}$$

$$H_{B4} = -2(1+\upsilon_{23}) g_{1,T}^{t} \left[\sum_{n=1}^{N} D_{n,T} e^{-\lambda_{n,T} \Delta \psi_{T}^{t}} q_{n,4}^{t-\Delta t} - D_{f,T} q_{f,4}^{t-\Delta t} \right] \tag{28-3}$$

$$H_{B5} = -g_{1,s}^{t} \left[\sum_{n=1}^{N} D_{n,S} e^{-\lambda_{n,s} \Delta \psi_{s}^{t}} q_{n,5}^{t-\Delta t} - D_{f,S} q_{f,5}^{t-\Delta t} \right] \tag{28-4}$$

$$H_{B6} = -g_{1,S}^{t} \left[\sum_{n=1}^{N} D_{n,S} e^{-\lambda_{n,s} \Delta \psi_{s}^{t}} q_{n,6}^{t-\Delta t} - D_{f,S} q_{f,6}^{t-\Delta t} \right] \tag{28-5}$$

where

$$\begin{aligned}
q_{n,i}^{t} &= e^{-\lambda_{n,T} \Delta \psi_{T}^{t}} q_{n,i}^{t-\Delta t} + \Gamma_{n,T} (g_{2,T}^{t} \sigma_{i}^{t} - g_{2,T}^{t-\Delta t} \sigma_{i}^{t-\Delta t}) && for\ i = 2,3,4 \\
q_{n,i}^{t} &= e^{-\lambda_{n,s} \Delta \psi_{s}^{t}} q_{n,i}^{t-\Delta t} + \Gamma_{n,s} (g_{2,s}^{t} \sigma_{i}^{t} - g_{2,s}^{t-\Delta t} \sigma_{i}^{t-\Delta t}) && for\ i = 5,6 \\
q_{f,i}^{t} &= q_{f,i}^{t-\Delta t} + 0.5 \Delta \psi_{T}^{t} (g_{2,T}^{t} \sigma_{i}^{t} - g_{2,T}^{t-\Delta t} \sigma_{i}^{t-\Delta t}) && for\ i = 2,3,4 \\
q_{f,i}^{t} &= q_{f,i}^{t-\Delta t} + 0.5 \Delta \psi_{S}^{t} (g_{2,S}^{t} \sigma_{i}^{t} - g_{2,S}^{t-\Delta t} \sigma_{i}^{t-\Delta t}) && for\ i = 5,6
\end{aligned} \tag{29}$$

After obtaining the three-dimensional incremental iteration form of the nonlinear viscoelastic constitutive equation, a user material subroutine (UMAT) in the ABAQUS FE code was implemented. Before predicting the creep deformation of the GFRP directors by FEM, a comparison of the numerical result and test result was carried out to verify the correctness of the viscoelastic parameters and the UMAT program. As shown in Fig. 6, the predicted results are in good agreement with the test data.

4.2 Finite element model for the creep response of launch canister

In a recent work (Yu et al. 2019), the authors detailed the assembly structure of the launch canister. The finite element model established in ABAQUS is an appropriate simplification of the real structure, mainly including GFRP directors, steel frame and rockets, as shown in Fig. 7. A total of 20

GFRP directors (4 rows and 5 columns) are clustered in the steel frame and their deformation is constrained by the frame. Otherwise, the deformation of the frame can also result in a forced deformation of the directors. Therefore, a complete finite element model of the launch canister is needed instead of an individual director model to study the creep response of the GFRP directors. The rocket was considered as discrete rigid body because the rocket is stiff and its deformation is not the object of current study. A lumped mass point is set at the barycenter of each rocket to give the actual mass of the rocket. The long-term creep behaviour of the steel frame was also considered and the material parameters were derived from previous work (Yu et al. 2019).

The GFRP director is an asymmetric thin-walled structure with a spiral groove and a large length to diameter ratio. The stacking sequence of the GFRP director is [90/(±53.7)/90], its nominal thickness is 2.5 mm, the nominal inner diameter is 120mm, and the nominal length is 3050 mm. The GFRP director was modelled using only one layer of 8-node isoparametric solid elements (C3D8) along the thickness direction, as shown in Fig. 8, while the steel frame was modelled using 8-nodel reduced-integration elements (C3D8R).

According to the actual assembly relationship, the connecting element was used to model the axial locking force between the rocket and the director. The surface to surface contact is defined between the bourrelet of the rocket and the inner face of the director, the guide lug of the rocket and the spiral groove of the director, the first and third positioning rings (the first positioning ring near the front of the launch canister) and the splints of the launch canister. Connection constraints were defined between the second and fourth positioning rings and the splints of the launch canister.

To meet the design requirements, the launch canister for three-layer stacking storage in the warehouse is appropriate for 10–15 years. The bottom of the launch canister must withstand both the weight of the various parts of the launch canister itself and the weight of the upper two launch canisters. Therefore, taking the bottom launch canister as the research object, from the perspective of saving computing resources, the weight of the above two launch canisters is simplified to a uniform pressure applied at the corresponding position. The boundary conditions are applied to the contact area between the bottom surface of the launch canister and the support pad (a special part for storage

of the launch canister). The applied load and boundary conditions are shown in Fig 7. Constrain the translational degrees of freedom for the four positioning holes on the bottom surface, U1=U3=0, and constrain the vertical degree of freedom for other areas contact with the stacking devices, U2=0.

Three analysis steps were set up to simulate stack loading, long-term storage creep, and removal of the above two launch canisters, respectively. The step time for the long-term storage creep analysis was 15 years and the maximum incremental time was 120 hours to ensure a sufficient calculation accuracy.

5 Results and discussion

5.1 Creep deformation of GFRP directors

The maximum residual deformation of all GFRP directors presents a saddle-shaped distribution in three-dimensional space after 15 years of stacking storage, as depicted in Fig. 9. The two directors in the middle of the upper and lower rows show a maximum residual deformation, while the two directors in the middle of the left and right columns show a minimum residual deformation. The maximum and minimum deformations are 0.24 mm and 0.22 mm, respectively.

A path is defined along the axial direction of the director with the largest residual deformation, and the residual deformation of each node on the path is depicted in Fig. 10. The maximum deformation position of the director is in the middle of the second and third positioning rings. There are two reasons to explain this phenomenon. First, the large distance between the second and third splints results in a lower stiffness of the director's section. The second reason is that the barycenter and both front and mid bourrelets of the rocket are located between the second and third splints.

The base director, located in the third row and third column, usually used as a reference to detect the parallelism of other directors, therefore, its residual deformation was output and presented in Fig.10. The maximum deformation of the base director is 0.22 mm, which smaller than the specified value of technical indicators

5.2 Influence of creep deformation on launching

Exploring the influence of creep deformation on rocket launching and evaluating the performance of the launch canister after long-term storage is the goal of creep deformation prediction. Therefore,

as a continuous research, we have established a projectile-barrel coupling launch dynamics model to compare the dynamic parameters of rocket launching before and after storage. The deformed mesh model was introduced into the new model as orphan mesh part and redefines the material properties and the interactions between parts. The director with the largest deformation was selected to simulate the launching process of the rocket.

According to the contact-collision force versus time curves shown in Fig. 11, the creep deformation of the director significantly increases the contact-collision force during launching. This is due to the creep deformation leading to a decrease in the clearance between the rocket and the director. The rocket's axial velocity versus time curves is presented in Fig. 12. We can see that after 15 years of storage, the rocket's run-off track velocity is declining. An increase in the contact-collision force increases the rocket's energy loss, resulting in a lower rocket velocity. The decrease of run-off track velocity will reduce the ability of rocket to resist external interference, which will affect the final firing dispersion.

6 Conclusions

This paper presented a complete process for predicting the long-term creep response of GFRP directors in multiple launch rocket systems, which is also applicable to other conventional composite structures. Furthermore, the influence of creep deformation on the dynamic parameters of rocket launch was also studied. The main conclusions can be summarized as follows:

(1) For the E-glass/epoxy 6509 composite, a nonlinear viscoelastic response appears when the transversely applied stress is higher than 26MPa, and the nonlinear viscoelasticity stress threshold in the shear direction is 15MPa.

(2) In the transverse direction, the value of nonlinear viscoelastic parameter g_{1T} increases as the stress level increases, and $a_{\sigma T}$ value decreases as the stress level increases, while the values of g_{0T} and g_{2T} are independent of the stress levels. All parameters in the transverse direction can be expressed by simple bi-linear functions of the average matrix octahedral shear stress.

(3) In the shear direction, the values of the nonlinear parameters g_{0S}, g_{1S} and g_{2S} increase with

increasing shear stress levels, while the $a_{\sigma S}$ values decrease with increasing shear stress levels. A sample bi-linear expression was used to fit the parameters g_{0S}, g_{1S} and $a_{\sigma S}$ as a function of the average matrix octahedral shear stress, while the $a_{\sigma S}$ parameter was fitted using an exponential function.

(4) Both parameters $a_{\sigma T}$ and $a_{\sigma S}$ are less than 1 and decrease with increasing stress levels, indicating that the stress promotes the viscoelastic response of the E-glass/epoxy 6509 composite. Therefore, a time-stress superposition principle (TSSP) can be used to develop the long-term creep compliance master curve based on short-term creep data.

(5) After 15 years of stacking storage, the maximum residual deformation of all GFRP directors presents a saddle-shaped distribution in three-dimensional space. The two directors in the middle of the upper and lower rows show a maximum residual deformation of 0.24 mm, and the two directors in the middle of the left and right columns show a minimum residual deformation of 0.22 mm.

(6) The creep deformation of the director results in a significant increase in the contact-collision force during launching, thereby reducing the run-off track velocity of the rocket.

Finally, it is well known that the viscoelastic properties of polymeric composites are significant affected by temperature and humidity. Therefore, in order to accurately predict the viscoelastic response of composite structures in actual service environment, it is necessary to develop a finite element model considering hygrothermal-mechanical coupling to predict the long-term creep response of composite structures, which is part of our future work.

Acknowledgments

The work presented in this paper has been funded by the Natural Science Foundation of Jiangsu Province (Grant No. BK20170837) and the Fundamental Research Funds for the Central Universities (No. 309181B8807)

References

Behzadpoor, H., Masoumi, S., Salehi, M. 2011. Micromechanical analysis of nonlinear viscoelastic unidirectional fiber-reinforced composites. Appl. Mech. Mater. **110-116**:1166-1170. doi:

10.4028/www.scientific.net/AMM.110-116.1166.

Chen, J.Z., Li, Z., Zhu, S.R., Li, Z.Q. 2013. Prediction of long-term properties of fiberglass pipe based on the shift factors method. Adv. Mater. Res. **748**:411-415. doi:10.4028/www.scientific.net/amr.748.411.

Dillard, D.A. 1981. Creep and creep rupture of laminated graphite/epoxy composites. Ph.D. thesis, Va. Tech, USA

Guedes, R.M. 2010. Nonlinear viscoelastic analysis of thick-walled cylindrical composites pipes. Int. J. Mech. Sci. **52**(8):1064-1073. doi: 10.1016/j.ijmecsci.2010.04.003.

Gramoll, K.C., Dillard, D.A.: Brinson, H.F. 1989. A stable numerical solution method for in-plane loading of nonlinear viscoelastic laminated orthotropic materials. Compos. Struct. **13**(4):251-274. doi:10.1016/0263-8223(89)90011-1.

Guedes, R.M. 2010. Creep and fatigue in polymer matrix composites. Woodhead Publishing in Materials.

Gallant, A.R. 1987. Nonlinear statistical models. John Wiley & Sons, New York.

Hiel C.C., Brinson H.F., Cardon A.H. 1983. The nonlinear viscoelastic response of resin matrix composites. Compos. Struct. **2**:271-281. doi: 10.1007/978-94-009-6640-6_20.

Haj-Ali, R.M., Muliana, A.H. 2004. A multi-scale constitutive formulation for the nonlinear viscoelastic analysis of laminated composites materials and structures. Int. J. of Solids. Struct. **41**(13):3461-3490. doi: 10.1016/j.ijsolstr.2004.02.008.

Huang, C.W., Masad, E., Muliana, A.H., Bahia, H. 2007. Nonlinearly viscoelastic analysis of asphalt mixes subjected to shear loading. Mech. Time-Depend Mat. **11**(2):91-110. doi: 10.1007/s11043-007-9034-5.

Japanese Standards Association, Tokyo. 1996. JIS K 7078-1996. Testing methods for tensile creep of carbon fiber reinforced plastics

Kennedy, T.C., Wang, M. 1994. Three-dimensional, nonlinear viscoelastic analysis of laminated composites. J. Compos. Mater. **28**(10):902-925. doi: 10.1177/002199839402801002.

Papanicolaou, G.C., Zaoutsos, S.P., Cardon, A.H. 1999. Further development of a data reduction

method for the nonlinear viscoelastic characterization of FRPs. Compos. Part A-Appl. S. **30**(7):839-848. doi: 10.1016/s1359-835x(99)00004-4.

Papanicolaou, G.C., Zaoutsos, S.P., Cardon, A.H. 1999. Prediction of the non-linear viscoelastic response of unidirectional fiber composites. Compos. Sci. Tech. **59**(9):1311-1319. doi: 10.1016/S0266-3538(98)00171-7.

Rariee, R., Mazhari, B. 2015. Modeling creep in polymeric composites: Developing a general integrated procedure. Int. J. Mech. Sci. **99**:112-120. doi: 10.1016/j.ijmecsci.2015.05.011.

Schapery, R.A. 1968. On a thermodynamic constitutive theory and its application to various nonlinear materials. Proceedings of IUTAM Symposium on Thermoinelasticity, East Kilbride, UK, 25-28, pp. 259-284.

Schapery, R.A. 1969. On the characterization of nonlinear viscoelastic materials. Polym. Eng. Sci. **9**(4):295-310. doi: 10.1002/pen.760090410.

Schapery, R.A. 1966. An engineering theory of nonlinear viscoelasticity with applications. Int. J. Solids. Struct. **2**:407–25. doi: 10.1016/0020-7683(66)90030-8.

Tuttle, M.E., Brinson, H.F. 1986. Prediction of the long-term creep compliance of general composite laminates. Exp. Mech. **26**(1):89-102. doi: 10.1007/BF02319961.

Yu, C.G., Li, Z.G. 2012. Analysis of rocket launching system. National Defence Industry Press, Beijing.

Yu, C.G., Sun, T.S., Xiao, G.Y. 2019. Study on creep performance of launch canister under long-term storage. T. Can. Soc. Mech. Eng. **43**(2):199-208. doi: 10.1139/tcsme-2018-0028.

Yang, T.Q., Luo, W.B., Wei, Y.T., Xu, P. 2004. Viscoelastic theory and its application. Science Press, Beijing.

Zaoutsos, S.P., Papanicolaou, G.C., Cardon, A.H. 1998. On the non-linear viscoelastic behaviour of polymer-matrix composites. Compos. Sci. Tech. **58**(6):883-889 doi: 10.1016/s0266-3538(97)00195-4.

Table 1. Elastic material properties for E-glass/epoxy lamina (average of five specimens)

E_1/GPa	E_2/GPa	G_{12}/GPa	X_t/MPa	Y_t/MPa	S/MPa	ν_{12}	ν_{23}
41.71	12.29	3.81	929.80	48.76	48.50	0.31	0.31

Table 2. Nonlinear viscoelastic parameters as a function of τ_{oct}

Parameters	Transverse direction		Shear direction	
	$\tau_{oct} \le 10.79$ MPa	$\tau_{oct} > 10.79$ MPa	$\tau_{oct} \le 12.55$ MPa	$\tau_{oct} > 12.55$ MPa
g_0	1.0	1.0	1.0	$\exp[0.0361(\tau_{\text{oct}} - 12.55)]$
g_1	1.0	$1.0+0.133(\tau_{\text{oct}} - 10.79)$	1.0	$1.0+0.0421(\tau_{\text{oct}} - 12.55)$
g_2	1.0	1.0	1.0	$\exp[0.104(\tau_{\text{oct}} - 12.55)]$
a_σ	1.0	$1.0-0.067(\tau_{\text{oct}} - 10.79)$	1.0	$1.0-0.0144(\tau_{\text{oct}} - 12.55)$

Table 3. Parameters for the linear-transient creep compliance

n	$\lambda_{n,T}$ (min^{-1})	$D_{n,T}$ (GPa^{-1})	$\lambda_{n,S}$ (min^{-1})	$D_{n,S}$ (GPa^{-1})	$D_{f,T}$ (GPa^{-1})	$D_{f,S}$ (GPa^{-1})
1	1	0.00152	1	0.0131	1.053E-07	2.495E-7
2	10^{-1}	0.000683	10^{-1}	0.00479		
3	10^{-2}	0.00152	10^{-2}	0.0135		
4	10^{-3}	0.00267	10^{-3}	0.0167		
5	10^{-4}	0.00169	10^{-4}	0.0231		
6	10^{-5}	0.00244	10^{-5}	0.0438		

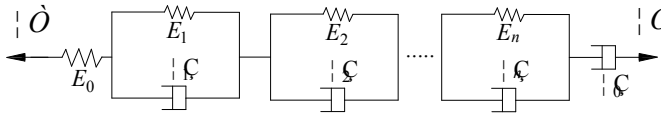

Fig. 1. Generalized Kelvin model

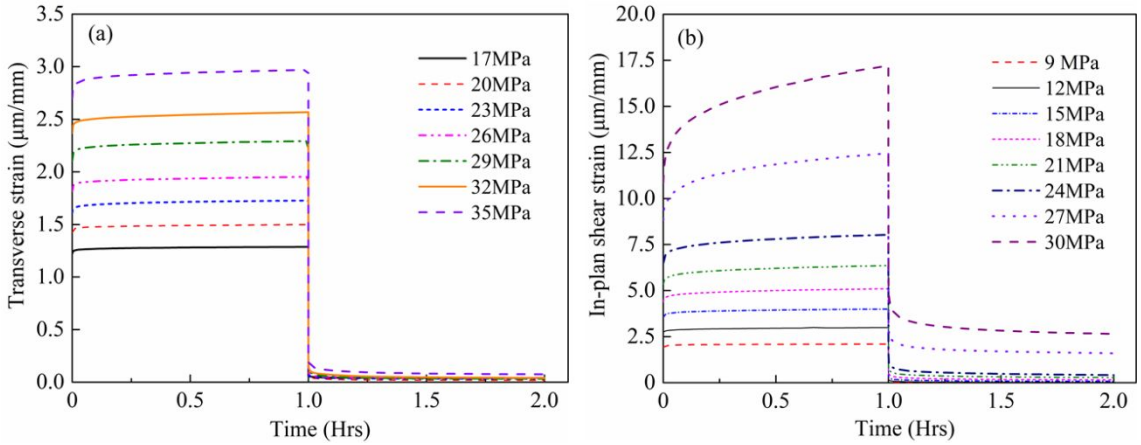

Fig. 2. 60/60-minute creep/creep-recovery strain versus time curves of GFRP at different stress levels:**(a)** Transverse direction; **(b)** Shear direction

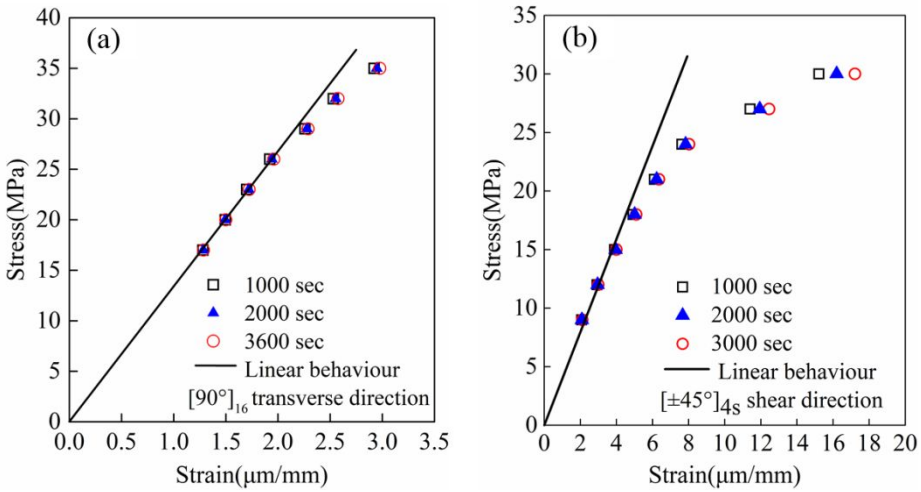

Fig. 3. Isochronous curves for transverse and shear directions at different time periods: **(a)** Transverse direction; **(b)** Shear direction

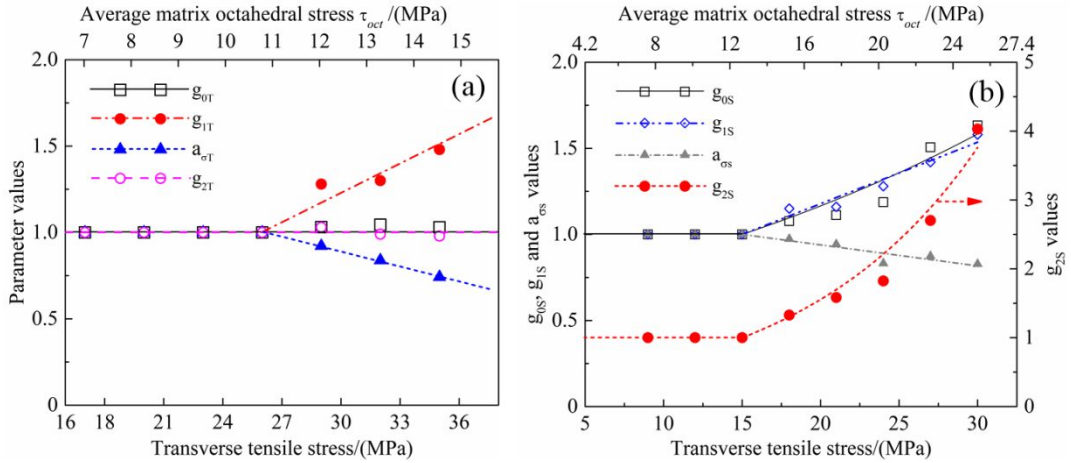

Fig. 4. Parameters as a functions of the applied stress and of the average matrix octahedral shear stress: **(a)** Transverse direction; **(b)** Shear direction

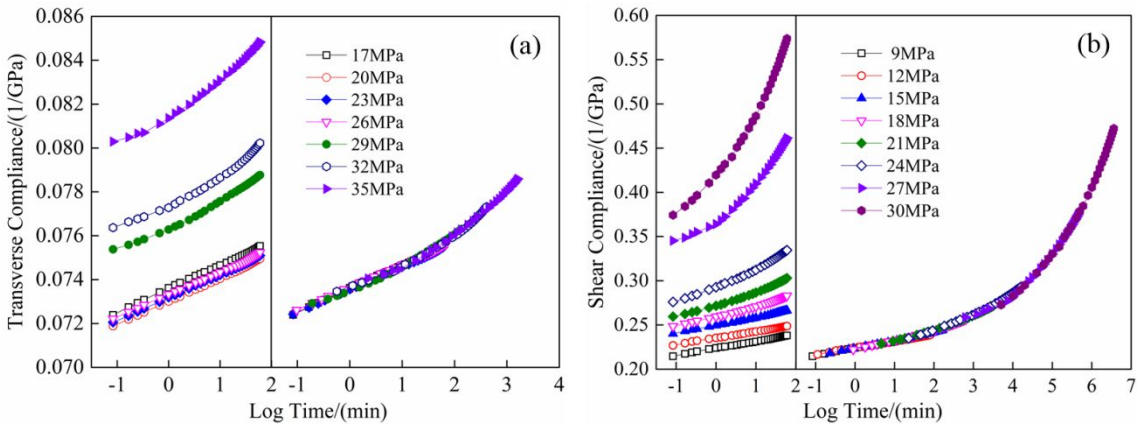

Fig. 5. Master curve of creep compliance for transverse and shear directions: **(a)** Transverse direction; **(b)** Shear direction

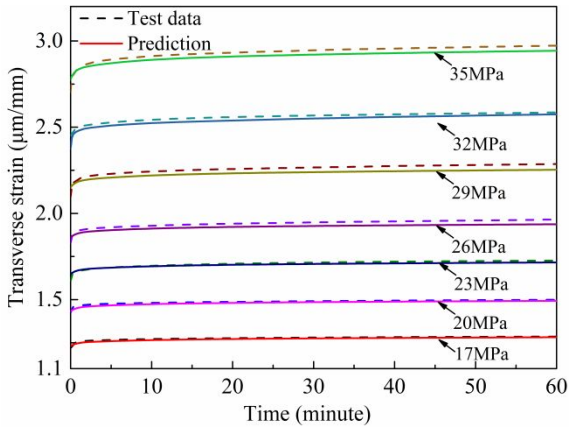

Fig. 6. Transverse creep strain for $[90]_{16}$ specimens

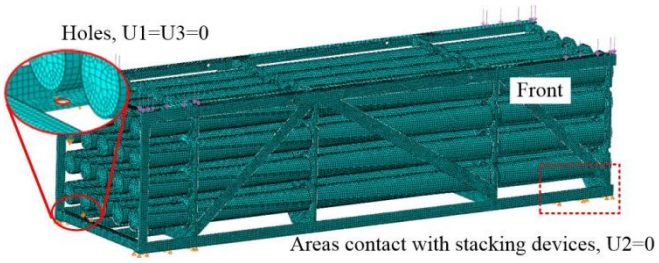

Fig. 7. Finite element model of the launch canister in ABAQUS

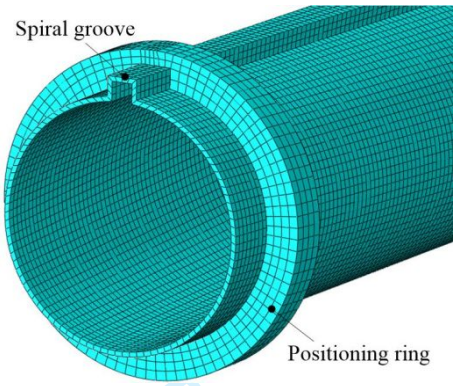

Fig. 8. Local view of GFRP director

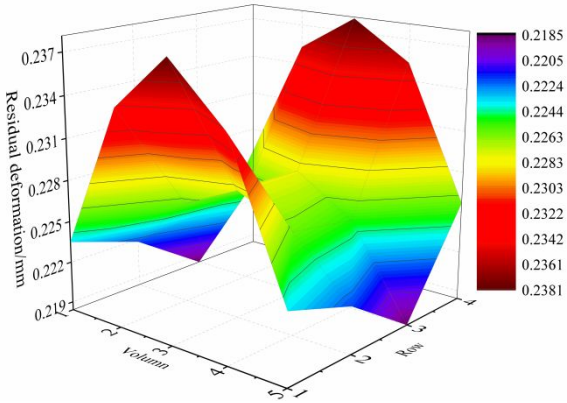

Fig. 9. Maximum residual deformation of directors

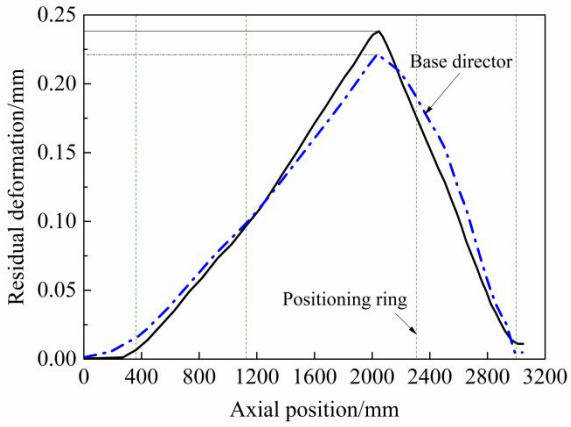

Fig. 10. Residual deformation of nodes in axial direction

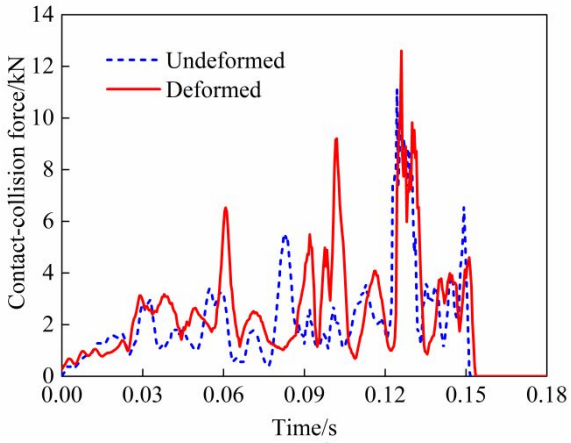

Fig. 11. Contact-collision force acting on the director

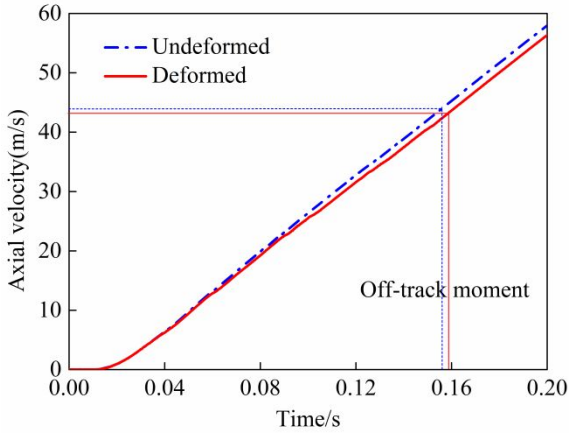

Fig. 12. Axial velocity versus time curves